

Vasiliki A. Mitsou<sup>ab</sup> for the ATLAS SCT Collaboration

<sup>a</sup> Instituto de Física Corpuscular (IFIC), CSIC – Universitat de València,  
Edificio Institutos de Investigación, P.O. Box 22085, E-46071 Valencia, Spain

<sup>b</sup> CERN, PH-ATT Department, CH-1211 Geneva 23, Switzerland  
vasiliki.mitsou@cern.ch

## Abstract

The SemiConductor Tracker (SCT) together with the Pixel detector and the Transition Radiation Tracker (TRT) form the central tracking system of the ATLAS experiment at the LHC. It consists of single-sided microstrip silicon sensors, which are read out via binary ASICs based on the DMILL technology, and the data are transmitted via radiation-hard optical fibres. After an overview of the SCT detector layout and readout system, the final-stage assembly of large-scale structures and the integration with the TRT is presented. The focus is on the electrical performance of the overall SCT detector system through the different integration stages, including the detector control and data acquisition system.

## I. INTRODUCTION

The ATLAS detector [1], one of the two general-purpose experiments of the Large Hadron Collider (LHC), has entered into the final stages of installation at CERN. The LHC, a proton-proton collider with a 14-TeV centre-of-mass energy and a design luminosity of  $10^{34} \text{ cm}^{-2}\text{s}^{-1}$ , is expected to deliver the first proton beam by the end of 2007. The ATLAS central tracker (Inner Detector, ID) [2] combines the silicon detector technology (pixels and micro-strips) in the innermost part with a straw drift detector with transition radiation detection capabilities (Transition Radiation Tracker, TRT) in the outside, operating in a 2-T superconducting solenoid.



Figure 1: Layout of the ATLAS Inner Detector: it comprises the Transition Radiation Detector, the Semiconductor Tracker and the Pixel system from the outer to the inner radii, respectively.

The microstrip detector (Semiconductor Tracker, SCT), as shown in Fig. 1, forms the middle layer of the ID between the Pixel detector and the TRT. The SCT system [2, 3] comprises a barrel made of four nested cylinders and two end-caps of nine disks each. The barrel layers carry 2112 detector units (*modules*)

altogether, while a total of 1976 end-cap modules are mounted on the disks. The whole SCT occupies a cylinder of 5.6 m in length and 56 cm in radius with the innermost layer at a radius of 27 cm.

The silicon modules [4, 5] consist of one or two pairs of single-sided *p-in-n* microstrip sensors glued back-to-back at a 40-mrad stereo angle to provide two-dimensional track reconstruction. The 285- $\mu\text{m}$  thick sensors [6] have 768 AC-coupled strips with an 80  $\mu\text{m}$  pitch for the barrel and a 57 – 94  $\mu\text{m}$  pitch for the end-cap modules. Between the sensor pairs there is a highly thermally conductive baseboard. Barrel modules follow one common design, while for the forward ones four different types exist according to their position in the detector.

## II. THE SCT READOUT SYSTEM

The readout of the module is based on 12 ABCD3TA ASICs manufactured in the radiation-hard DMILL process mounted on a copper/kapton hybrid [7]. The ABCD3TA chip [8] features a 128-channel analog front end consisting of amplifiers and comparators and a digital readout circuit operating at a frequency of 40.08 MHz. This ASIC utilises the binary scheme where the signals from the silicon detector are amplified, compared to a threshold and only the result of the comparison enters the input register and a 132-cell deep pipeline, awaiting a level-1 trigger accept signal. It implements a redundancy mechanism that redirects the output and the control signals, so that a failing chip can be bypassed. To reduce the channel-to-channel threshold variation, in particular after irradiation, the ABCD3TA features an individual threshold correction in each channel with a 4-bit digital-to-analog converter (*TrimDAC*) with four selectable ranges. In addition, a calibration circuitry is implemented in the chip providing an injection charge in the range 0.5 – 10 fC. By injecting various known charges and performing threshold scans, the analogue properties of each channel can be determined, such as the gain, the offset and the noise.

The clock and command signals as well as the data are transmitted from and to the off-detector electronics through optical links [9]. On the detector side, the DORIC<sup>1</sup> and VDC<sup>2</sup> are utilised for receiving the optical clock and control signal (one link) and for data transmission (two links), respectively. Therefore, three optical fibres are connected to each module, terminated by an opto-package consisting of Si *p-i-n* diodes and VCSELs mounted on the Back-Of-Crate (BOC) card. The latter serves as an interface between the optical signals and the off-detector electronics in the Read-Out Driver (ROD). Each ROD

<sup>1</sup>Digital Optical Receiver Integrated Circuit.

<sup>2</sup>VCSEL (Vertical Cavity Surface Emitting Laser) Driver Chip.

controls and monitors 48 SCT modules.

The LHC operating conditions demand challenging electrical performance specifications for the SCT modules and the limitations mainly concern acceptable noise occupancy level, tracking efficiency, timing and power consumption. These requirements reflect on the design of the readout system, as well as on the quality assurance/control strategy followed throughout the detector construction. To this respect, a series of electrical tests were performed during the various stages of the detector assembly; from module production [10], to macro-assembly [11], at reception at CERN [12], and eventually after the final integration with TRT. These repetitive tests are necessary to ensure that the module/system performance does not change after each stage, to finalise the corresponding data acquisition software, and to learn how to recover potential errors/problems. The final stages of the SCT assembly and testing at CERN were carried out in the ATLAS SR1 clean-room, equipped with a system capable of characterising up to one million readout channels simultaneously. Electronics tests results such as electrical connections checks, noise and gain measurements, as well as temperature and leakage current measurements were given particular attention. The outcome of these electronics tests, essential also for the validation of the grounding, shielding and cooling system, are discussed in the following sections.

### III. SCT ASSEMBLY AND INTEGRATION

After the module production, being distributed over several sites in Australia, Europe, Japan and the USA, the macro-assembly<sup>3</sup> took place in three laboratories, in the UK and the Netherlands. The four barrel layers were assembled at the University of Oxford employing two specially designed robots for the mounting of modules onto cylindrical support structures. A detail of a barrel layer showing the overlapping modules is given in Fig. 2 (left). The on-detector services, being fitted during macro-assembly, include thin-wall Cu-Ni pipes and module cooling blocks, which remove heat through an evaporative C<sub>3</sub>F<sub>8</sub> cooling system. The modules are individually supplied with LV and HV power through Al- or Cu-on-Kapton low mass tapes.

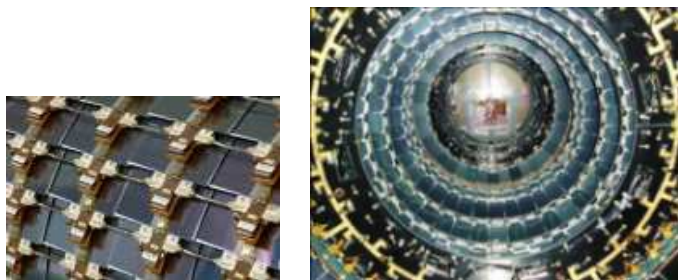


Figure 2: Left: detail from a barrel outer surface; silicon sensors and hybrids are visible. Right: beam's eye view of end-cap C.

The electrical performance of whole barrels was duly tested in Oxford for barrels 3, 4 and 6<sup>4</sup> and at CERN for barrels 3 and 5. All digital and analog functions were examined by following standard measuring procedures [10]. The tests showed

stable operation for a simultaneous readout of up to one million channels in terms of thermal operation, data acquisition and detector control. More than 99.7% of all barrel channels are fully operational as evident from Table 1, where detailed information for dead and noisy channels for each barrel is given. These figures are in agreement with the ones obtained during module production. The average module noise was stable at  $4.5 \times 10^{-5}$ , well below the design specification of  $5 \times 10^{-4}$ . Concerning the detector bias, the leakage current drawn by the sensors at  $\sim 15^\circ\text{C}$  was much lower than  $1 \mu\text{A}$  at the nominal bias value of 150 V, *i.e.* within the specifications.

Table 1: Channel defects breakdown for the barrel SCT as measured after macro-assembly, in Oxford and at CERN.

Barrel	Total nr. channels	Dead	Noisy	Other	Total defects
B3	589 824	357	460	666	1483 (0.25%)
B4	737 280	245	242	354	841 (0.11%)
B5	884 736	770	492	556	1818 (0.21%)
B6	1 032 192	2513	1936	1271	5720 (0.55%)
Total	3 244 032	3885	3130	2847	9862 (0.30%)

After completing the individual testing of the barrels at CERN SR1 room, the four layers were eventually integrated into one barrel. This operation, completed within a period of three months, was carried out step-by-step with one layer being inserted into the structure each time from the largest down to the smallest one. During this operation, the SCT services of the *inner* layer were transferred onto a horizontal service support structure, whereas the ones of the *outer* layer were unfolded radially at the ends.

The two end-caps, on the other hand, were brought together at the University of Liverpool (End-Cap C, *EC-C*) and at NIKHEF (End-Cap A, *EC-A*). The modules were manually mounted onto disks, fully characterised in a test-box and finally the disks were installed inside carbon fibre cylinders. A photograph of the fully assembled *EC-C* as seen from inside is shown in Fig. 2 (right); all disks are clearly visible. Both end-caps have been transferred to CERN —first *EC-C* and then *EC-A*— and they have passed successfully the reception tests, which include visual inspection, disk alignment measurements, examination of the cooling circuits and comprehensive electronics tests. The *EC-A* was tested while cooled down to the nominal temperature of  $-7^\circ\text{C}$  in contrast to *EC-C* which was tested warm. The measured ENC<sup>5</sup> noise for each module of *EC-A* is shown in Fig. 3. These values are comparable to the ones measured during module assembly [10] and after macro-assembly at NIKHEF. The fraction of dead channels was also found to be at the same level as previously measured and around 0.2%.

Many of the activities performed on the SCT large structures was devoted to connection and manipulation of services, *i.e.* the connection of the evaporative cooling plants, the final power supplies and readout electronics. A prototype of the final Data Acquisition (DAQ) system, consisted of RODs and BOCs, and

<sup>3</sup>Mounting of modules onto disks (end-cap) or cylinders (barrel) and installation of the respective services.

<sup>4</sup>The four SCT barrels are numbered from 3 to 6 starting from the innermost one, *i.e.* B3–B6, whereas B0–B2 denote the pixel layers.

<sup>5</sup>Equivalent Noise Charge defined as the input charge giving signal equal to effective output noise (expressed in electrons).

the Detector Control System (DCS) was engaged. The DCS provides high and low voltage for the sensors and ABCD3TA chips, voltage for the DORIC and VDC ASICs and monitors the temperature on the modules. Besides monitoring and controlling various parameters of these power supplies, the DCS includes a hard-wired interlock system which automatically switches off the power supply to certain groups of modules in the event of an over-temperature. In addition, the DCS monitors humidity and temperature sensors mounted on the outlets of each cooling loop and records the corresponding data.

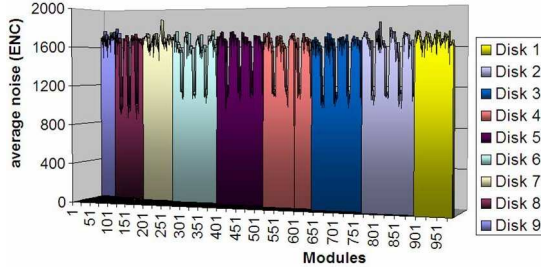


Figure 3: ENC noise per module for all disks of end-cap A as measured at CERN. The modulation observed in the plot is due to the different noise levels of the four types of end-cap modules [5];  $\sim 1450 - 1550 e^-$  for the outer and long middle modules and  $\sim 900 - 1100 e^-$  for the inner and short middle ones.

Each of the three SCT blocks, the barrel and the end-caps, are enfolded in cylindrical structures, the Outer and the Inner Thermal Enclosures (OTE and ITE, respectively). These foam-based layers, covered by aluminised Kapton (OTE) or carbon-fibre-reinforced-plastic (ITE), provide gas tightness,<sup>6</sup> thermal isolation and Faraday shielding. The gas envelopes are complemented by flat panels fitted on the ends. A quite large fraction of testing time was given to gas tightness measurements, identification and sealing of leaks. After several iterations, the leak rate was reduced to an acceptable level for the barrel and EC-C (EC-A OTE has not been fitted yet).

#### IV. BARREL SCT-TRT INTEGRATION

The integration and commissioning of the barrel SCT with the respective TRT [14] is almost complete. It started in February 2006 with the insertion of one detector into the other, shown in Fig. 4, using a rail system and a cantilever stand. During this operation, the SCT services were transferred onto the Insertion Service Support Structure (ISSS), fixed onto the SCT cradle extensions. The TRT, installed in the inner detector trolley, was finally slid over the SCT.

A series of combined tests followed the integration of the barrel ID, covering a wide spectrum of operational and detector performance related aspects [15]. During these tests in SR1, one eighth of the TRT and one quarter of the SCT were equipped with the complete readout chain, in a top-bottom layout as shown in the left-hand side of Fig. 5. As far as the SCT is concerned, 468 out of the 2112 modules were read out using 12 RODs and one TIM.<sup>7</sup> In the TRT, on the other hand, about 10 000 channels were examined with nine RODs and three

TTCs. Three scintillator counters were also installed (see Fig. 5, left) to provide an external trigger from cosmic rays to both detector systems. A typical cosmic-ray track is shown on the right-hand side of Fig. 5 as reconstructed by a combined SCT & TRT tracking algorithm. The measurement results that follow were obtained with this *cosmic* setup.



Figure 4: Insertion of barrel SCT into barrel TRT; the OTE is visible surrounding the barrel SCT, as well as the services on the ISSS (foreground).

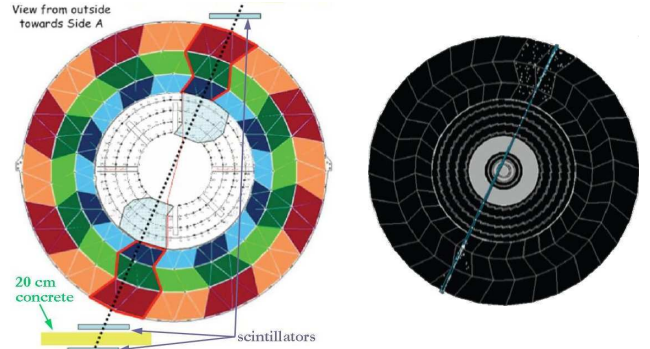


Figure 5: Left: Transverse schematic view of the setup for the cosmic run. The actually read out parts are highlighted (half of the bottom TRT section was not read out). Three scintillator counters were used for trigger. Right: reconstructed cosmic track in the SCT and the TRT.

A typical electrical testing sequence begins by establishing communication between the modules and the off-detector electronics system and by optimising the optical links settings. After the digital tests, *i.e.* checking the redundancy links, the chip by-pass functionality and the pipeline circuit, the analogue measurements follow. These include measurements of the gain, the offset and the noise for each channel and evaluation of the module noise occupancy. The noise is measured by performing a threshold scan in the absence of charge injection. The slope of the logarithm of the occupancy versus the square of the threshold is approximately proportional to the ENC noise. Furthermore, the noise occupancy at the 1-fC threshold level is obtained, with the exact 1-fC point for each channel already been defined by the trimming. Several distinct configurations were tried in order to assess the potential dependence of the noise on those.

The noise stability was monitored throughout the measurements and only a slight increase was observed for single barrels in comparison with the macro-assembly values, as well as between the whole barrel and the individual barrel layers. No pick-up noise was detected in the presence of external heaters

<sup>6</sup>The SCT will be operated in a  $N_2$  environment at  $-7^\circ C$ , whereas the TRT will be embedded in  $CO_2$  at a temperature of  $\sim 20^\circ C$ .

<sup>7</sup>TTC (Timing, Trigger & Control) Interface Module.



on the SCT thermal enclosure. After applying temperature corrections, the ENC noise was found to be  $\sim 40 - 50 e^-$  higher for the barrel than after macro-assembly.

For the noise occupancy measurements, the TrimDAC thresholds for each channel were initially set to the value obtained during module production, leading however to a wide threshold variation. To remedy this problem the so-called *new Response Curve (RC)* configuration was introduced, which included a  $\sim 10\%$  wafer-by-wafer correction to account for variations in the ABCD3TA calibration capacitor. The latter configuration is compared with the *old trim target* uncorrected one in Fig. 6 with respect to the measured noise occupancy. With the new configuration, the noise occupancy values are clearly less scattered, returning an r.m.s. value of  $3.7 \times 10^{-5}$ , whereas the old one gives an r.m.s. of  $5.5 \times 10^{-5}$ . The observed decrease in the mean value with the RC threshold, on the other hand, is due to the long period of detector bias preceding these measurements, rather than the threshold configuration. This behaviour had previously been observed in single barrel tests and is evident in calibration as well as physics-mode runs. The RC configuration was used throughout the cosmic run.

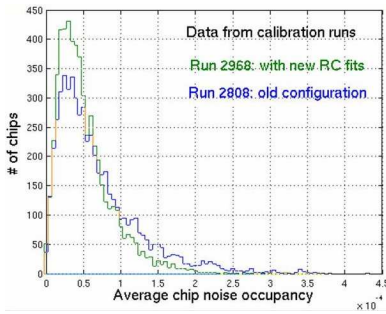


Figure 6: Average noise occupancy for each chip for the cosmic test setup and for two different threshold configurations: the ‘old trim target’ (blue), rendering a mean (r.m.s.) value of  $6.8 \times 10^{-5}$  ( $5.5 \times 10^{-5}$ ), and the ‘new RC’ (green), returning  $5.1 \times 10^{-5}$  ( $3.7 \times 10^{-5}$ ), respectively. The measurements with RC configuration were taken after a few days with detector bias.

The effect of high trigger frequency was studied by varying the pulser rate in physics mode. For a trigger rate ranging from 5 Hz up to 50 kHz, no evidence of increase in noise occupancy was found.

The grounding scheme may be a potential factor contributing to noise level. Therefore the effect of a change in the grounding was studied, by measuring the noise occupancy with the power supply DC shorting cards *in* and *out* when noth SCT and TRT are triggered from a pulser at 50 Hz. No significant change in the noise occupancy was observed, however the grounding scheme in SR1 is not the final one, which will not be available before the detector is installed in its final position.

Noise can be evaluated by two methods: online with calibration scans and triggers provided by the ROD and TIM and offline with physics mode runs triggered by a pulser by applying the offline analysis. With either approach practically the same results were obtained in terms of noise occupancy.

<sup>8</sup>In view of the foreseen 1% strip occupancy on any event, data compression is employed, in order to reduce the number of bits of data read out of the chip for each event. This logic examines the three bits of data, representing three beam crossings centred on the level-1 trigger time, making up the hit pattern for each channel. The state ‘X’ denotes any bit value; 0 or 1.

In Fig. 7, a comparison between the ENC noise recorded when the SCT only is read out (left panel) and when the TRT is also operated simultaneously (right panel). The ENC noise in both cases remains the same and equal to  $\sim 1750 e^-$ , thus no electrical pick-up noise is induced between the two detectors. A similar result is acquired when a different data compression logic<sup>8</sup> than the previously applied *test mode* (XXX, excluding 000) is selected; for the *level mode* (X1X), the ENC noise is 1611 electrons for the SCT only and 1610 electrons for SCT & TRT together. Similar conclusions are drawn for the TRT in the absence/presence of the SCT readout.

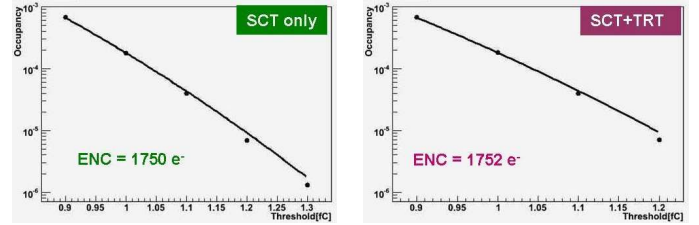


Figure 7: Noise occupancy as a function of the threshold for SCT only (left panel) and for SCT and TRT simultaneous readout (right panel) when the *test mode* (XXX, excluding 000) is selected for the data compression. The points represent measurements taken with threshold scans and the curves are analytically (through a complementary error function) derived from the ENC value indicated.

As far as common-mode noise is concerned, no evidence of such was found. There was no increase in noise occupancy observed when using synchronous triggers. No correlations have been observed neither between noise hits within chips, nor between hits on different modules.

The ID barrel was transported from SR1 building and installed in the ATLAS detector in August 2006. After being lowered into the ATLAS cavern with only a few millimeters of clearance, the detector was successfully inserted in the liquid argon calorimeter cryostat (see Fig. 8). The final stage of the barrel ID commissioning is under way, involving the connection of cables and services, the verification of full connectivity to the power supplies, readout and DAQ systems, and the on-detector functionality checks of all detector modules for SCT and TRT. This intervention will be carried out by implementing the final grounding and shielding scheme for all  $\sim 2000$  SCT modules and the complete TRT. It should validate the detector for autonomous operation for ten years without further access.



Figure 8: The barrel ID installed in its final position inside the electromagnetic calorimeter cryostat bore.

## V. END-CAP SCT-TRT INTEGRATION

The integration of the forward parts of the ID started in September 2006 with the insertion of the SCT EC-C into the TRT EC-C, shown in Fig. 9. Before this operation, the functionality of an octant of the EC-C was successfully tested inside the thermal enclosures. The readout and power cables are currently being connected in preparation for the two-month long combined tests in the SR1 clean-room. During those, one quadrant of the SCT, *i.e.* 247 modules, will be read out together with an adjacent sector of the TRT corresponding to 1/16 of the total end-cap (7680 straws/channels).



Figure 9: Insertion of the SCT EC-C into the TRT EC-C.

The ID EC-A, on the other hand, is going to follow more or less the same integration and installation steps as EC-C. However, this process is expected to proceed faster taking advantage of the experience gained during the EC-C integration. The ID EC-A is expected to be integrated by November. Both end-caps are scheduled to be ready for installation in the ATLAS cavern by January – February 2007.

## VI. CONCLUSIONS

ATLAS SCT is progressing well towards integration with the other parts of the ID, installation in ATLAS and commissioning. Repeated tests in various stages have demonstrated operational stability and good electrical performance. The fraction of dead channels has been kept below 0.2%. Particular attention was given to the electronics tests such as electrical connections checks, noise and gain measurements, as well as temperature and leakage current measurements. The outcome of these tests validated the grounding, shielding and cooling system. As far as noise is concerned, no remarkable change with respect to measurements during module production and macro-assembly has been observed and no pick-up noise has been detected while TRT is read out. Combined tests with cosmic rays allowed to gain experience with the overall operational and running conditions (DAQ, DCS, monitoring, *etc.*). The barrel ID (SCT & TRT) has been successfully installed in the ATLAS cavern inside the electromagnetic calorimeter cryostat and the SCT end-caps integration with the TRT has already started and is well under way. The innermost layer of the ID, the Pixel detector, will be installed independently in 2007.

## ACKNOWLEDGMENTS

The progress reported in this paper represents work performed across the ATLAS SCT collaboration. I would like to thank all my colleagues whose work is presented here and, in particular, Pepe Bernabeu for his useful comments and suggestions.

## REFERENCES

- [1] ATLAS Collaboration, ATLAS Technical Proposal, CERN/LHCC/94-43 (1994); <http://atlas.web.cern.ch/Atlas/>
- [2] ATLAS Collaboration, Inner Detector Technical Design Report vol. I & II, CERN/LHCC/97-16 & CERN/LHCC/97-17 (1997).
- [3] *For a recent review see:* Z. Dolezal, Nucl. Phys. Proc. Suppl. **150** (2006) 128.
- [4] A. Abdesselam *et al.*, Nucl. Instrum. Meth. A **568** (2006) 642 [ATL-INDET-PUB-2006-005].
- [5] A. Abdesselam *et al.*, “The ATLAS semiconductor tracker end-cap module,” Nuclear Instruments and Methods in Physics Research A (2007), doi:10.1016/j.nima.2007.02.019.
- [6] D. Robinson *et al.*, Nucl. Instrum. Meth. A **485** (2002) 84; A. Ahmed *et al.*, “The Silicon Microstrip Sensors of the ATLAS Semiconductor Tracker,” submitted to Nuclear Instruments and Methods A.
- [7] Y. Unno, Proc. 11th Workshop on Electronics for LHC and Future Experiments (LECC 2005), Heidelberg, Germany, 12–16 September 2005 (2005), pp. 11–15.
- [8] F. Campabadal *et al.*, Nucl. Instrum. Meth. A **552** (2005) 292.
- [9] A. Abdesselam *et al.*, “The ATLAS SCT Optoelectronics and the Associated Electrical Services” [ATL-INDET-PUB-2007-001], submitted to Nuclear Instruments and Methods A.
- [10] V. A. Mitsou, IEEE Trans. Nucl. Sci. **53** (2006) 729 [arXiv:physics/0606263].
- [11] G. Viehhauser, Conference Record of the 2004 IEEE Nuclear Science Symposium, Rome, Italy, 16–22 October 2004 (2004), pp. 1188–1191.
- [12] B. Mikulec, Conference Record of the 2005 IEEE Nuclear Science Symposium, El Conquistador Resort, Puerto Rico, 23–29 October 2005 (2005), pp. 1480–1484.
- [13] H. Sandaker, Nucl. Instrum. Meth. A **541** (2005) 96; ATLAS SCT Collaboration, “The ATLAS SCT Detector Readout and Data Acquisition,” in preparation.
- [14] T. Akesson *et al.*, Nucl. Instrum. Meth. A **522** (2004) 25; **522** (2004) 50; **522** (2004) 131.
- [15] M. J. Costa, “Cosmics and Final ATLAS ID-SCT Tests,” contributed to 2006 IEEE Nuclear Science Symposium (NSS), San Diego, California, 29 October – 4 November 2006.